

different, with greater energy being required to stretch the bonds with the larger  $\pi$  bond order than to compress the pair with weaker  $\pi$  bonding.

The stabilization energy of 3.1 kcal/mol, computed for lengthening just one set of bonds in the radical cation while holding the other set fixed at the optimal length for the square geometry, is still considerably more than the stabilization energy of only 1.0 kcal/mol that is calculated for rhomboidal distortion. This finding suggests that in the radical cation derived from tetra-*tert*-butylcyclobutadiene, a rectangular distortion should still remain preferable to a rhomboidal one, although the energy difference between the two might well be smaller than in the parent radical cation.

#### Comparison with Cyclobutadiene

Although electron repulsion complicates carrying out *calculations* on the radical cation, electron repulsion plays a much smaller role in the *behavior* of this species than in the neutral molecule. This is due, of course, to the fact that one of the two nonbonding electrons in cyclobutadiene is absent in the radical cation. Consequently, the radical cation behaves just as one would expect from inspection of the degenerate Hückel MO's (Figure 2), with distortions from square to both rectangular and rhomboidal geometries being favorable. The calculated preference for the former over the latter can be understood from the nodal patterns in the MO's that are appropriate for describing each of the distorted structures and the fact that  $\pi$  interactions between nearest neighbor atoms are more important than those between atoms diagonally across the four-membered ring.

In contrast, in the ground state of the neutral molecule a rhomboidal distortion is unfavorable,<sup>3,4</sup> since it requires placing both nonbonding electrons in one of the  $\pi$  MO's that is localized to two atoms along a diagonal plane of symmetry. Minimization of electron repulsion in square cyclobutadiene actually causes only

one of the nonbonding electrons to occupy each of these MO's;<sup>11</sup> therefore, the ground state of the square molecule is incapable of profiting from a rhomboidal distortion. Consequently, unlike the radical cation, which can pseudorotate from one rectangular minimum to another via a rhomboidal geometry, the neutral molecule cannot avoid passing through a square transition state.

Electron repulsion in the neutral molecule is also responsible for the fact that the energy lowering, computed at the  $\sigma$ - $\pi$  CI level, for distortion from a square to a rectangular geometry is very similar for both the neutral molecule and the radical cation. The stabilization energies are similar, despite the presence in the neutral molecule of one more electron in the  $e_g$   $\pi$  orbitals that induce the distortion. Although the additional electron does result in cyclobutadiene being predicted to have a more rectangularly distorted equilibrium geometry than the radical cation,<sup>1-4</sup> in the neutral molecule rectangular distortion from a square increases the Coulombic repulsion energy between the pair of nonbonding  $\pi$  electrons.<sup>11</sup> This increase partially cancels the energy lowering due to the stronger  $\pi$  bonding (in the Hückel sense) at the rectangular equilibrium geometry of the neutral molecule.

If  $\pi$  bonding, which is maximized at a rectangular geometry, is disrupted by lengthening the strong  $\pi$  bonds or shortening the weak ones, the neutral molecule tends toward a square geometry in order to minimize the Coulomb repulsion energy between the nonbonding electrons.<sup>7</sup> In contrast, in the radical cation, where only one nonbonding electron is present, this effect is absent. Consequently, unlike the case in the neutral molecule, the two sets of bond lengths in the radical cation are independent of each other. This is the physical origin of the difference in behavior that is predicted by eq 1 and 2 and confirmed computationally by the results of our *ab initio* calculations.

**Acknowledgement** is made to the donors of the Petroleum Research Fund, administered by the American Chemical Society, and the National Science Foundation for support of this work.

## Location and Relative Orientation of Methanol Adsorbate Molecules in A, X, and Y Zeolites from Electron Spin-Echo Studies

M. Narayana and Larry Kevan\*

*Contribution from the Department of Chemistry, University of Houston, Houston, Texas 77004. Received December 15, 1980*

**Abstract:** Hydroxymethyl radicals have been generated by  $\gamma$ -radiolysis at 77 K from specifically deuterated methanols, CD<sub>3</sub>OH and CH<sub>3</sub>OD, adsorbed on NaA, Ca<sub>4</sub>Na<sub>4</sub>A, NaX, KX, NaY, and KY zeolites. These radicals have been studied by electron spin-echo spectrometry and the deuterium modulation patterns analyzed. In A zeolites, the hydroxymethyl radical is located in the  $\alpha$ -cage above a hexagonal interior face, with the molecular radical's electric dipole oriented along the threefold axis of the hexagonal face. Since a majority of the cations are in or near the hexagonal faces this orientation is consistent with a cation charge-molecular dipole interaction controlling the adsorbate geometry. The radical interacts with three equivalent closest methanol molecules in the  $\alpha$ -cage, with their methyl groups 0.38 nm from the  $\alpha$ -carbon of the radical. The radical location and orientation in X and Y zeolites is similar, except that both square and hexagonal faces are involved and the three nearest interacting methanol molecules lie slightly further away.

Zeolites are hydrated aluminosilicates with a cage structure and are widely used for sorption and catalysis.<sup>1</sup> A variety of investigations have been conducted into the thermodynamics and kinetics of sorption of various materials on synthetic zeolites. Electron spin resonance studies<sup>2-5</sup> have yielded some information

on interactions between adsorbed molecular radicals and zeolitic interior surfaces. However, the continuous wave methods used in most electron spin resonance experiments are not very suitable for studying the weak interactions between a paramagnetic center and adsorbate molecules or with the lattice nuclei. Even though some crystal structure information is available, relatively little

(1) Rabo, J. A. In "Zeolite Chemistry and Catalysis"; Rabo, J. A., Ed.; American Chemical Society: Washington, D.C., 1976.

(2) Sohma, J.; Shiotani, M. In "Magnetic Resonance in Colloid and Interface Science"; Resing, H. A., Wade C. G., Ed.; American Chemical Society: Washington, D.C., 1976; Vol. 34, p 141.

(3) Wang, K. M.; Lunsford, J. J. *Phys. Chem.* 1970, 74, 1512.

(4) Katsu, T.; Yanagita, M.; Fujita, Y. *J. Phys. Chem.* 1970, 74, 580.

(5) Huang, Y.; Vansant, E. F. *J. Phys. Chem.* 1973, 77, 663.

is known about the sorption sites in zeolites.

Recently, the power and usefulness of pulsed methods like electron spin-echo modulation analysis for studying weak hyperfine interactions have been amply demonstrated.<sup>6-8</sup> Dikanov et al.<sup>9</sup> and Ichikawa and Kevan<sup>10</sup> have generated the hydroxymethyl radical,  $\text{CH}_2\text{OH}$ , from adsorbed methanol on A, X, and Y zeolites and have detected hyperfine interactions with  $^{27}\text{Al}$  nuclei by electron spin-echo methods. Some results have also been obtained on the orientation of the hydroxymethyl radical relative to methanol molecules in the same cage in A zeolites. Here we present more comprehensive results on hydroxymethyl radical orientations and interactions in the cages of A, X, and Y zeolites carried out by electron spin-echo studies using specifically deuterated methanol molecules.

### Zeolite Structure

All three zeolites used in the present study, A, X, and Y, are cubic in structure but differ in silicon-to-aluminum ratio and in the way the sodalite units are coupled. A sodalite unit is a truncated octahedron formed by silica and alumina tetrahedra, with eight hexagonal and six square faces. In the X and Y zeolites each sodalite unit is tetrahedrally coupled to four other units through hexagonal prisms. The space within the sodalite unit is called the  $\beta$ -cage and the space encompassed by the coupled sodalite units is called the super cage or  $\alpha$ -cage. The cation sites with a high occupancy probability are: site I in the center of hexagonal prisms, site I' also in the hexagonal prisms but somewhat displaced toward the  $\beta$ -cage, site II in the center of hexagonal openings of the sodalite units into the  $\alpha$ -cage, site II' slightly displaced from the center of hexagonal openings into the  $\beta$ -cages, and site III in the square faces of hexagonal prisms in the  $\alpha$ -cage also involving square faces of the sodalite units. Linde 13X, a typical X zeolite, has  $\sim 85$  sodium ions while a Y zeolite like Linde YZ-52 has  $\sim 54$ . X-ray diffraction studies indicate that 16 of the sodium ions occupy site I in hexagonal prisms. About 24 more occupy site II in hexagonal windows and the rest are not locatable by X-ray diffraction. In NaX it has been further suggested that site II occupation is dependent on the aluminum content of the zeolite.<sup>11</sup> The occurrence of three aluminums per hexagonal window is thought to be necessary to cause partial dehydration thus rendering site II energetically favorable for a cation to occupy.

On dehydration of the zeolite, some of the exchangeable cations appear to migrate<sup>12</sup> from site I to site I' and from unlocatable sites to sites II, II', and III. Especially in dry monovalent cation Y zeolites, the site II occupancy seems to be high as inferred from infrared studies.<sup>13</sup>

The structure of A zeolites is somewhat simpler.<sup>14</sup> Eight sodalite units are arranged at the corners of a cube and are coupled together by small cubes called double four-rings. The body diagonals of the cube are also the threefold axes of the hexagonal windows. In the primitive cell, there are twelve exchangeable monovalent cations per unit cell. Eight of them are on the body diagonals close to the hexagonal window centers (site S2). In NaA, three of the other four occupy positions close to the center of eight-ring windows of the  $\alpha$ -cage (site S5) and the 12th ion is located near a four-ring site in the  $\alpha$ -cage (site S3). Site S2 in A zeolites is similar to site II in X and Y zeolites. In the case of commercially available 5A zeolite,  $\text{Ca}_4\text{Na}_4\text{A}$ , all of the eight

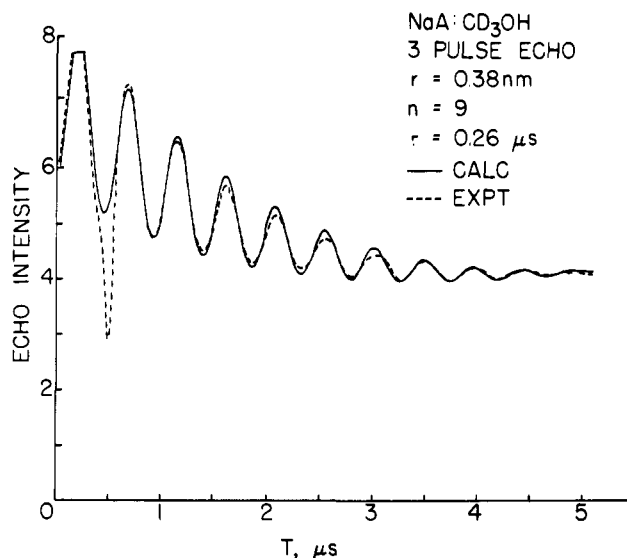


**Figure 1.** Comparison of experimental (···) and calculated (—) three-pulse electron spin-echo deuterium modulation for  $\text{CD}_2\text{OH}$  in NaA zeolite. The decay function used is  $\exp(2.20 - 0.291T + 0.042T^2 - 0.002T^3)$ .

cations are on threefold axes on or near the hexagonal windows.

### Experimental Section

Using Linde 3A, 4A, 5A, 13X, and YZ-52 zeolites the following cationic forms were prepared: NaA,  $\text{Ca}_4\text{Na}_4\text{A}$ , NaX, KX, NaY, and KY. The exchange was carried out at  $80^\circ\text{C}$  with use of 1 M solutions of the required cations. Three exchanges were made to ensure adequate exchange of the cation.

The zeolites were placed in 3 mm o.d. spectroil quartz tubes and dehydrated under vacuum for 10 h at 373 K to a residual pressure of  $2 \times 10^{-6}$  torr and for 20 h at 623 K to the same residual pressure.  $\text{CD}_3\text{OH}$  and  $\text{CH}_3\text{OD}$  (Stohler Isotope Chemicals Inc.) were thoroughly degassed and adsorbed onto the zeolites at the saturated vapor pressure at room temperature for 2 h. The samples were then cooled to 77 K, briefly evacuated, and sealed. The  $\gamma$ -irradiation was done with a  $^{60}\text{Co}$   $\gamma$  source at 77 K to a maximum dose of 0.3 Mrad.

Electron spin-echo spectra were recorded on a home-built spectrometer<sup>15</sup> at 4.2 K. Pulses of 50 ns width and 100 W power were used to record both the primary (2-pulse) and stimulated (3-pulse) echoes.

### Theory

In a two-pulse spin-echo experiment  $90^\circ$  and  $180^\circ$  pulsed separated by a time interval  $\tau$  are applied to the spin system and the echo is observed at time  $\tau$  after the second pulse. In a three-pulse experiment, two  $90^\circ$  pulses separated by time  $\tau$  are followed by a time  $T$  after which a third  $90^\circ$  pulse is applied which stimulates an echo produced  $\tau$  after the third pulse. The echo decay envelope is often modulated by interaction with surrounding nuclei, the theory of which has been extensively described.<sup>5-8</sup> The data reduction method involving a ratio analysis has been described in detail.<sup>16</sup> From a comparison of theoretical and experimental ratios, the number of nuclei contributing to the modulation pattern,  $n$ , their distance to the paramagnetic center,  $r$ , and the isotropic hyperfine coupling,  $a_{\text{iso}}$ , can be determined. The parameter  $n$  is constrained to be integral and can typically be uniquely determined up to about  $n = 10$ . For larger values of  $n$  the uncertainty is about 10%. The parameter  $r$  can normally be determined to  $\pm 0.01$  nm and  $a_{\text{iso}}$  to  $\pm 15\%$  for good quality data. The simulated modulation patterns are directly compared with the experimental curves by using a general decay function of the type

$$g(T) = \exp(A_0 + A_1T + A_2T^2 + A_3T^3) \quad (1)$$

for three-pulse echo data where the coefficients are determined by a least-squares method.<sup>16</sup>

(15) Ichikawa, T.; Kevan, L.; Narayana, P. A. *J. Phys. Chem.* **1979**, *83*, 3378.

(16) Ichikawa, T.; Kevan, L.; Bowmann, M.; Dikanov, S. A.; Tsvetkov, Yu. D. *J. Chem. Phys.* **1979**, *71*, 1167.

(6) Mims, W. B. *Phys. Rev.* **1972**, *B5*, 2409.

(7) Kevan, L. In "Time Domain Electron Spin Resonance"; Kevan, L., Schwartz, R. N., Ed.; Wiley-Interscience: New York, 1979; Chapter 8.

(8) Mims, W. B. In "Electron Paramagnetic Resonance"; Geschwind, S., Ed.; Plenum: New York, 1972; Chapter 4.

(9) Dikanov, S. A.; Yudanov, V. F.; Samoilov, R. I.; Tsvetkov, Yu. D. *Chem. Phys. Lett.* **1977**, *52*, 520.

(10) Ichikawa, T.; Kevan, L. *J. Am. Chem. Soc.* **1980**, *102*, 2650.

(11) Olson, D. H. *J. Phys. Chem.* **1970**, *74*, 2758.

(12) Strome, D. H.; Kleier, K. *J. Phys. Chem.* **1980**, *84*, 981.

(13) Butler, W. M.; Angell, C. L.; McAllister, W.; Risen, N. M. *J. Phys. Chem.* **1977**, *81*, 2061.

(14) Yanagida, R. Y.; Amaro, A. A.; Seff, K. *J. Phys. Chem.* **1973**, *77*, 805.

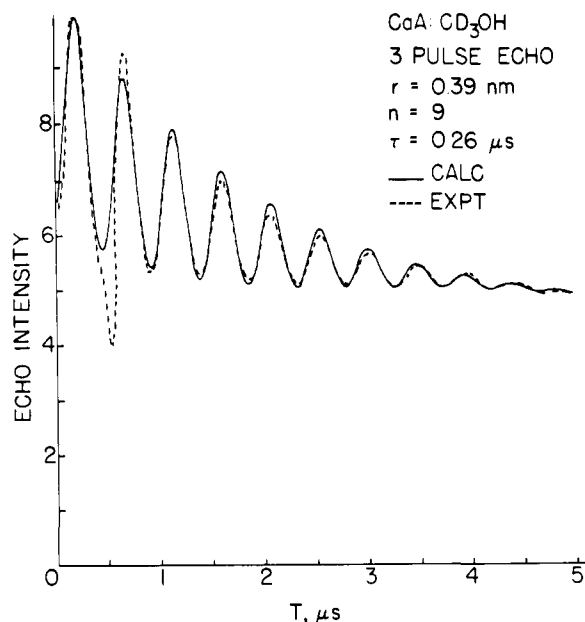


**Figure 2.** Comparison of experimental (---) and calculated (—) three-pulse electron spin-echo deuterium modulation for  $\text{CD}_2\text{OH}$  in  $\text{Na}_4\text{Ca}_4\text{A}$  zeolite. The decay function used is  $\exp(2.36 - 0.252T + 0.048T^2 - 0.004T^3)$ .

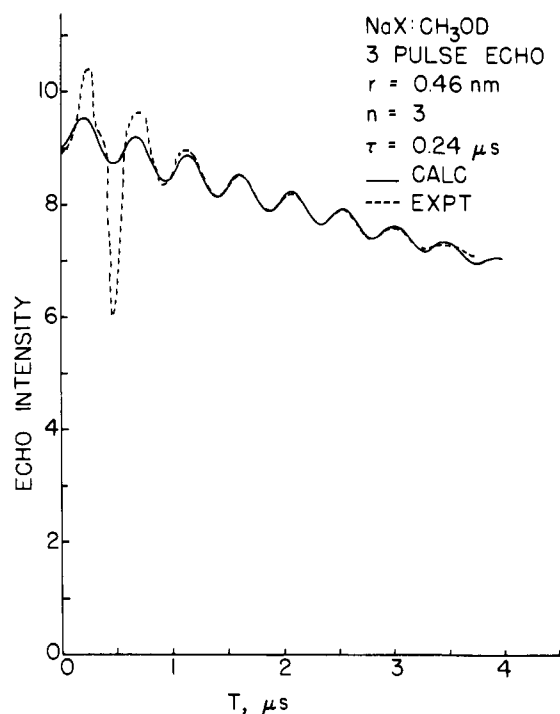


**Figure 3.** Comparison of experimental (---) and calculated (—) three-pulse electron spin-echo deuterium modulation for  $\text{CH}_2\text{OD}$  in NaX zeolite. The decay function is  $\exp(2.28 - 0.075T)$ .

### Results

In all samples the formation of the hydroxymethyl radical was verified by recording the echo-induced ESR by keeping  $\tau$  constant and sweeping the magnetic field. The electron spin-echo spectra are recorded on the high-field line to minimize the contributions from other paramagnetic species such as the  $\text{Na}_4^{3+}$  center.<sup>17,18</sup> Figures 1–5 show deuterium modulations for  $\text{CD}_2\text{OH}$  and  $\text{CH}_2\text{OD}$  in NaA,  $\text{Ca}_4\text{Na}_4\text{A}$ , NaX, KX, and KY zeolites. The spectra were analyzed by using the ratio analysis method described earlier and

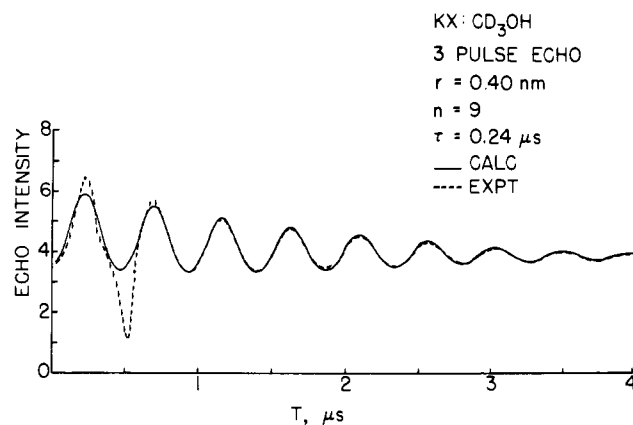


**Figure 4.** Comparison of experimental (---) and calculated (—) three-pulse electron spin-echo deuterium modulation for  $\text{CD}_2\text{OH}$  in KX zeolite. The decay function used is  $\exp(1.82 - 0.165T + 0.048T^2 - 0.005T^3)$ .

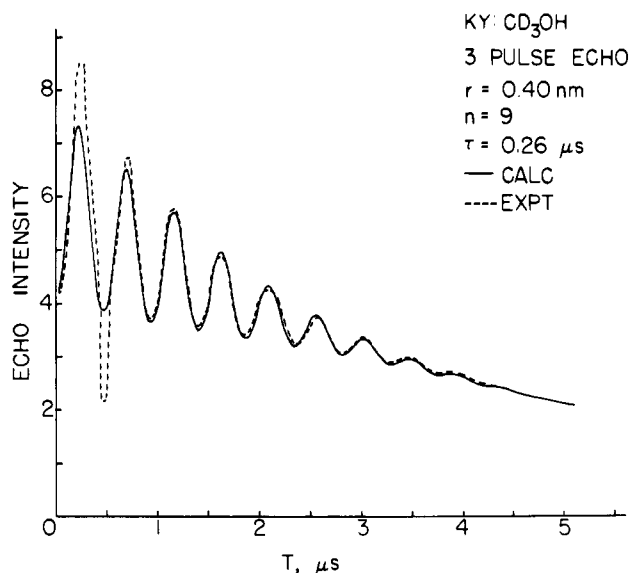


**Figure 5.** Comparison of experimental (---) and calculated (—) three-pulse electron spin-echo deuterium modulation for  $\text{CD}_2\text{OH}$  in KY zeolite. The decay function used is  $\exp(2.52 - 0.134T)$ .

the parameters determined are given in the figures. In X and Y zeolites the  $\text{CD}_2\text{OH}$  radical was found to interact with nine deuterons indicating three methanol molecules at 0.40–0.42 nm. In A and X zeolites the  $\text{CH}_2\text{OD}$  radical interacts with three deuterons at 0.47 nm. This is also consistent with three neighboring methanol molecules.

### Discussion

Since hydrogen bonding and charge-dipolar interaction are two of the important mechanisms involved in sorption, one can start with the probable cation positions as likely sorption sites for the adsorbed molecules. Our results seem consistent with the model shown in Figure 6. The  $\alpha$ -cage in NaA can be described by a cube with a 1.2 nm body diagonal and with a  $\text{Na}^+$  at each corner. In the case of full saturation with methanol about eight molecules are adsorbed in the  $\alpha$ -cage.<sup>9</sup> These can be arranged one on each side of the four body diagonals as shown in Figure 6. This arrangement is such that the methanolic oxygen is 0.20 to 0.25 nm above a hexagonal face with the molecular dipole oriented along the body diagonal. The molecular dipole of  $\text{CH}_3\text{OH}$  is along the bisector of the COH angle.<sup>19</sup> Then the paramagnetic center (unpaired electron on the carbon of the radical) is 0.32 to 0.37 nm from the hexagonal face, 0.30 to 0.35 nm from the center of the  $\alpha$ -cage, and 0.36 to 0.41 nm from other methyl groups. This

(17) Kasai, P. H. *J. Chem. Phys.* **1965**, *43*, 3322.

(18) Ben Taarit, Y.; Naccache, C.; Che, M.; Tench, A. *J. Chem. Phys. Lett.* **1973**, *24*, 41.

(19) Ivash, E. V.; Dennison, D. M. *J. Chem. Phys.* **1973**, *21*, 1804.

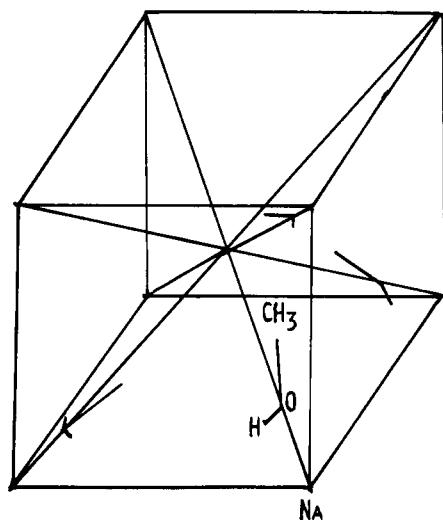


**Figure 6.** Model for the relative orientation of methanol molecules in A zeolite. The cube represents the  $\alpha$ -cage with each corner being a  $\text{Na}^+$  in a hexagonal window. The arrangement by which a hydroxymethyl radical interacts with three nearest methanol molecules is shown.

is in good agreement with our experimental distance of 0.38 nm to the adjacent methyl groups. It can be seen from Figure 6 that a radical in this position would have only three other nearest methanol molecules at the same distance, two on adjacent body diagonals and one immediately above or below itself. This also agrees with our experimental result of three adjacent molecules.

In A zeolites our results are in agreement with those of Dikanov et al.<sup>9</sup> in the distance between the radical site and methyl groups on adjacent molecules. However, they conclude that there are only two methanol molecules adjacent to the radical whereas our data indicate three molecules. We believe the accuracy of our data analysis clearly distinguishes between two and three adjacent molecules.

In the geometrical model of Figure 6 the experimental inter-methyl group distance determines a radical site-to-cation distance of  $\sim 0.35$  nm. The sodium modulation cannot be isolated from that of aluminum because their Larmor frequencies are too close. So we studied the electron spin-echo of hydroxymethyl radicals in LiA zeolite. Preliminary results from an analysis of lithium modulation indicate a cation-to-radical site distance of 0.38 nm which is in good agreement with the model of Figure 6.

Figure 7 bears on the orientation of the hydroxymethyl radical with respect to a hexagonal face of the  $\alpha$ -cage. In Figure 7A the methanol molecules are shown with their molecular dipoles oriented along threefold axes perpendicular to the hexagonal faces. If the C-O direction, instead of the molecular dipole direction, were to be placed along the threefold axis, as in Figure 7B, the distance from the radical site to the hexagonal face of the  $\alpha$ -cage is still 0.35 nm, but the distance to the adjacent methyl groups would only be 0.29 nm, which is significantly less than the experimental result of 0.38 nm. Furthermore, this gives a radical oxygen-to-sodium distance of 0.2 nm which results in a lattice oxygen-to-hydroxyl proton distance of 0.17 nm which is shorter than expected for hydrogen bonds in zeolites. Figure 7C shows the CO direction of the radical tilted  $50$ – $60^\circ$  from the threefold axis so that the molecular dipole is approximately oriented toward the  $\text{Na}^+$ . This gives a more satisfactory lattice oxygen-to-hydroxyl proton distance of 0.3 nm and a  $\text{CH}_3$ -to- $\text{CH}_3$  distance between adjacent methanol molecules of 0.35–0.41 nm which agrees well with experiment.

Dikanov et al.<sup>9</sup> suggested a spherical model in which the methanol molecules are arranged along the radii of a sphere representing that  $\alpha$ -cage with the methyl groups at 0.23–0.33 nm from its center. In this model the radical interacts with only two other methyl groups at 0.40 nm, but it appears that they have neglected the methanol molecule in the octant below or above the octants containing the radical. While this distance is consistent with our results, the number of neighbors is not. Another dif-

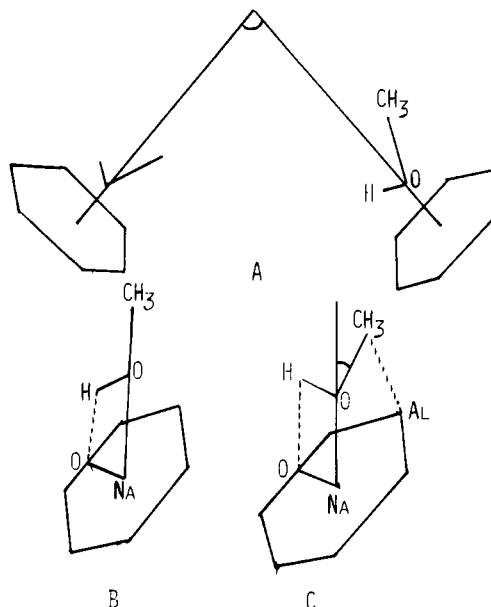


**Figure 7.** Orientation of the methanol molecule adsorbed in A, X, and Y zeolites with respect to the hexagonal windows of the  $\alpha$ -cage: (A) Two adjacent body diagonals which are also threefold axes in A zeolite are shown with the molecular dipole of the methanol molecule oriented along them. (B) Radical orientation if the C-O bond is aligned along the threefold axis of a hexagonal window. The distances are not compatible with the experimental results. For the  $\text{Na}^+$ -to-radical oxygen distance of 0.20–0.25 nm the lattice oxygen-to-hydroxyl proton distance is 0.17 nm, which is too short, and the  $\text{CH}_3$ -to- $\text{CH}_3$  distance between adjacent methanol molecules is 0.3 nm, which also is too short. (C) For the same  $\text{Na}^+$ -to-radical oxygen distance of 0.20–0.25 nm but with the CO bond of the radical making a  $50$ – $60^\circ$  angle with the threefold axis, the lattice oxygen-to-hydroxyl proton distance is  $\sim 0.3$  nm and the  $\text{CH}_3$ -to- $\text{CH}_3$  distance between adjacent methanol molecules is 0.35–0.41 nm, which is in good agreement with experiment.

ference is the cation-to-radical site distance. The methanolic oxygen in the model of Dikanov et al.<sup>9</sup> was fixed at 0.15 nm from the  $\alpha$ -cage surface while at the same time the radical site-to-cation distance was given as  $>0.45$  nm. However, according to the first constraint this distance would be about 0.30 nm from the C-O bond length since the cations in NaA are almost in the plane of the hexagonal windows. So there seems to be some inconsistency. Dikanov et al.<sup>9</sup> arrived at the radical site-to-cation distance of  $>0.45$  nm by a comparison of aluminum modulations in NaA and CaA. Here, it should be pointed out that the contribution of one  $^{23}\text{Na}$  ( $I = 3/2$ ) would in any case be small compared to that of three  $^{27}\text{Al}$  ( $I = 5/2$ ) nuclei from the hexagonal window since the modulation depth is proportional to the nuclear spin as well as to the number of nuclei. We have carried out electron spin-echo studies in  $\text{Cu}^{2+}$  doped LiA,  $\text{Cs}_7\text{Na}_5\text{A}$ ,  $\text{Rb}_{11}\text{Na}_1\text{A}$ , and T1A zeolites<sup>20</sup> in addition to the hydroxymethyl radical studies. The results indicate that the depth of modulation from aluminum depends on the type of cation present, presumably through the quadrupole interaction due to the electric field gradient at the site of the aluminum ions. Thus, conclusions based on comparisons of aluminum modulations might be complicated.

In the X and Y zeolites the cations are in the hexagonal prisms (site I), in or near the hexagonal windows (site II) between the  $\alpha$ - and  $\beta$ -cages, and near the square faces (site III) in the  $\alpha$ -cage. The cations in site I are in unfavorable positions as far as methanol molecules are concerned since they are too large to enter the  $\beta$ -cages. Even though the site I cations can still interact with adsorbed molecules in the  $\alpha$ -cage through the square faces of the hexagonal prisms, this influence is expected to be negligible compared to that of cations in sites II and III. Thus the hexagonal windows and square faces of the sodalite units are the most probable sorption sites.

(20) Narayana, M.; Kevan, L., 1980, unpublished results.

By constructing a model of X and Y zeolites we find that on either of these sites a methanol molecule will have three nearest neighbors at about 0.4 nm if the methanolic oxygen is located  $\sim 0.25$  nm above the square or hexagonal faces with the molecular dipole pointing toward the center of the face. This is in good agreement with our experimental results and 0.25 nm is a reasonable distance for coordination of the oxygen to a cation in the square or hexagonal face. This model indicates a cation-to-radical site distance of 0.38–0.40 nm. Spin-echo studies of hydroxymethyl radicals in CsX, CsY, LiX, and LiY zeolites have also been made.<sup>20</sup> In these studies the modulation from the cation could be clearly seen and the analysis indicates a cation-to-radical site distance of 0.40–0.45 nm. This again is in agreement with our model.

For a hydrogen bond between the hydroxyl proton and a lattice oxygen to be not too weak, the molecular dipole has to be tilted away from the threefold axis of a hexagonal face or the fourfold axis of a square face. A tilt of 5–10° seems to be reasonable as shown in Figure 7C and such an arrangement explains the 0.47-nm distance obtained from the analysis of deuterium modulation in CH<sub>3</sub>OD adsorbed X zeolites. Modulation is not seen from the  $\alpha$ -deuterons on the radical itself because the hyperfine coupling is so large that conditions for producing modulation are not met.<sup>7</sup>

In our earlier paper on hydroxymethyl radicals in X, Y, and A zeolites, the aluminum modulations were interpreted on the basis of the Al/Si ratio in these zeolites.<sup>10</sup> Accordingly, a radical situated above a square or hexagonal face of the  $\alpha$ -cage in line with a lattice Al(Si) ion was shown to interact with 0.4, 0.3, or 0.5 Al ions as determined by the factor  $n_{\text{Al}}/(n_{\text{Al}} + n_{\text{Si}})$  in the lattice of X, Y, and A zeolites. However, unless the radical is flipping between the Al and Si ion sites, one radical would interact with Al and another with Si and their contributions to the net echo

decay would be additive.<sup>21</sup> Hence the modulation amplitude should be

$$V_{\text{mod}} = \frac{n_{\text{Si}}}{n_{\text{Si}} + n_{\text{Al}}} V_1 + \frac{n_{\text{Al}}}{n_{\text{Si}} + n_{\text{Al}}} V_2$$

and not  $(V)^{n_{\text{Al}}/(n_{\text{Al}}+n_{\text{Si}})}$  as given earlier.<sup>10</sup> However, the number of aluminum ions interacting with the radical would still be governed by Al/Si ratio. This is because the first term would only contribute to the decay and not to the modulation since the Si nuclei have zero nuclear spin.

### Conclusions

From the analysis of modulations observed in the echo decay curves of hydroxymethyl radicals in A, X, and Y zeolites information about the location and relative orientation of methanol molecules in these zeolites is obtained. In A zeolites the hydroxymethyl radical is located in the  $\alpha$ -cage above a hexagonal window with the molecular dipole oriented along the threefold axis. It interacts with three other equivalent closest methanol molecules in the  $\alpha$ -cage with their methyl groups at 0.38 nm from the radical site. In X and Y zeolites the radical is also located in the  $\alpha$ -cage above a hexagonal window or square face and interacts with three equivalent closest methanol molecules at 0.40–0.42 nm. A model consistent with these numbers and distances is proposed.

**Acknowledgment.** This research was supported by the Department of Energy and the National Science Foundation. We thank Dr. R. Janakiraman for helpful discussions.

(21) Tsvetkov, Yu. D.; Dikanov, S. A., 1979, private communication.

## Mechanism of Oxidation of an Amine Coordinated to Ruthenium

Michael J. Ridd and F. Richard Keene\*

*Contribution from the Department of Chemistry and Biochemistry, James Cook University of North Queensland, Townsville, Queensland 4811, Australia. Received November 17, 1980*

**Abstract:** The mechanism of the oxidative dehydrogenation of  $[\text{Ru}(\text{bpy})_2\text{ampy}]^{2+}$  (bpy = 2,2'-bipyridine; ampy = 2-(aminomethyl)pyridine) to the corresponding imine complex has been studied in aqueous media by using stopped-flow methods in association with chemical oxidation by Ce(IV), flash photolysis techniques, and electrochemical methods. Solutions to the rate laws for several possible mechanisms were obtained numerically and the spectrophotometric responses matched with the theoretical solutions by use of a nonlinear optimization program. The data were found to be consistent with a mechanism involving a Ru(IV) species in which the ampy ligand is deprotonated, and this intermediate subsequently undergoes a two-electron transfer (accompanied by deprotonation) to give the imine product. The various rate constants for the individual steps of the mechanistic scheme were consistent with values for electron-transfer reactions and proton equilibria in similar metal complex systems.

The oxidative dehydrogenation of amines to imines or nitriles is known to be catalyzed by their coordination to metal centers. Initial studies of the oxidation of macrocyclic amines were made by Curtis<sup>1</sup> and Busch,<sup>2</sup> and recent studies<sup>3,4</sup> have confirmed the earlier assertion<sup>2</sup> that such reactions involved initial oxidation of the metal center followed by an intramolecular redox process in

which the ligand is oxidized and the metal reduced.

The analogous oxidation of coordinated ethylenediamine to the corresponding  $\alpha,\alpha'$ -diimine has also been reported,<sup>5-7</sup> and Meyer et al.<sup>8</sup> and Ford et al.<sup>9</sup> have studied the oxidation of a range of bidentate amines coordinated to ruthenium. The oxidative de-

(1) Curtis, N. F. *Coord. Chem. Rev.* **1968**, *3*, 3–47 and references therein.

(2) Goedken, V. L.; Busch, D. H. *J. Am. Chem. Soc.* **1972**, *94*, 7355–7363.

Hipp, C. J.; Lindoy, L. F.; Busch, D. H. *Inorg. Chem.* **1972**, *11*, 1988–1994.

(3) Maruthamuthu, P.; Patterson, L. K.; Ferraudi, G. *Inorg. Chem.* **1978**, *17*, 3157–3163.

(4) Jaacobi, M.; Meyerstein, D.; Lilie, J. *Inorg. Chem.* **1979**, *18*, 429–433.

(5) Beattie, J. K.; Elsbernd, H. *J. Chem. Soc. A* **1970**, 2598–2600.

(6) Lane, B. C.; Lester, S. E.; Basolo, F. *Chem. Commun.* **1971**, 1618–1619.

(7) Goedken, V. L. *J. Chem. Soc., Chem. Commun.* **1972**, 207–208.

(8) Brown, G. M.; Weaver, T. R.; Keene, F. R.; Meyer, T. J. *Inorg. Chem.* **1976**, *15*, 190–196.

(9) Alvarez, V. E.; Allen, R. J.; Matsubara, T.; Ford, P. C. *J. Am. Chem. Soc.* **1974**, *96*, 7686–7692.